Direct Observation of Molecular Orbitals of Pentacene Physisorbed on Au(111) by Scanning Tunneling Microscope

W.-H. Soe,[1] C. Manzano,[1] A. De Sarkar,[1] N. Chandrasekhar,[1] and C. Joachim[1,2]
[1]*IMRE, A*STAR (Agency for Science, Technology and Research), 3 Research Link, 117602, Singapore*
[2]*CEMES, CNRS, 29 rue Jeanne Marvig, 31055 Toulouse Cedex, France*
(Received 27 November 2008; published 1 May 2009)

Differential conductance (dI/dV) images taken with a low-temperature scanning tunneling microscope enabled the first observation of the electron probability distribution of the molecular orbitals of a pentacene molecule directly adsorbed on a metal surface. The three highest occupied molecular orbitals (HOMO, HOMO-1, and HOMO-2) and the lowest unoccupied molecular orbital are imaged. Thus dI/dV imaging without any intervening insulating layer permits the visualization of a large variety of molecular orbitals in the electronic cloud of a wide-gap molecule physisorbed on a metal surface.

DOI: 10.1103/PhysRevLett.102.176102 PACS numbers: 68.37.Ef, 68.43.−h

A molecule placed between two electrodes of a tunnel junction increases the junction conductance, since the electron cloud of the molecule lowers the effective tunnel barrier of the junction as compared to an empty junction vacuum barrier. However, the molecule retains its electronic resonances corresponding to its ionized or reduced states when coupled weakly to the metal electrodes. These are usually described by an antisymmetric product of one electron eigenstate, the so-called molecular orbitals. Assuming the validity of Koopmans theorem [1] in a tunnel junction environment, it has been shown [2] that it is possible to image the electron probability distribution in real space of the two pentacene frontier molecular orbitals (MOs). However, the surface preparation required for such an experiment is complex. It consists of separating the molecule from the metal surface using an ultrathin insulating layer [2–4]. The drawback of this technique is that the electron residence time in the tunneling junction increases when compared to the geometry where the molecule is directly adsorbed on the metal surface. This induces dynamic electrostatic effects which significantly alter the molecular orbital energies, with respect to the substrate Fermi level [5]. Even if the energy gap between MOs can be reduced, the energy window to image the MO of a selected resonance is consequently narrowed with this surface preparation, since the molecule is more likely to jump onto the tip apex or be destroyed by the resulting high electric field. To have access to more MOs, we return to a bare metal surface and physisorb the molecule of interest. We show in this Letter that aside from the two frontier MOs [i.e., the highest occupied molecular orbital (HOMO) and lowest unoccupied molecular orbital (LUMO)], the second (HOMO-1) and third (HOMO-2) occupied MOs of a pentacene molecule lying directly on a gold surface can be imaged using a scanning tunneling microscope (STM) via differential conductance measurements.

For the experiments reported here, pentacene molecules were sublimed on a Au(111) single crystal substrate, at room temperature. The surface was cleaned by repeated cycles of sputtering and annealing. Subsequently the sample was cooled to cryogenic temperatures and transferred to an STM chamber. All the images and spectroscopic data were acquired in an ultrahigh vacuum ($\leq 10^{-10}$ mbar) with a Createc low-temperature STM operated at 6 K. After sublimation, pentacene molecules adsorb on the Au(111) reconstructed terraces and at step edges. Even at large tunneling resistances, the molecules are prone to be dragged by the STM tip during image acquisition.

Imaging the MOs requires tunneling resistances in the order of hundreds of megohms. Only pentacene molecules physisorbed at herringbone kinks (as presented in Fig. 1) are used for recording spectroscopic data and dI/dV maps,

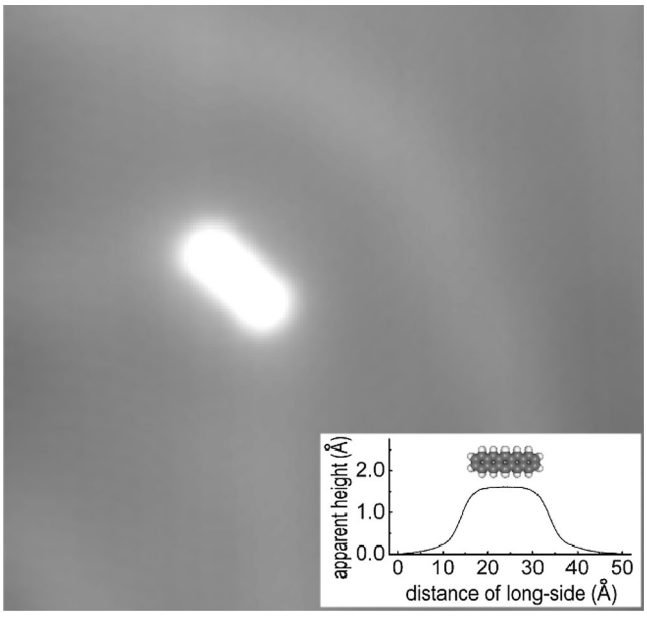

FIG. 1. A 10.0 nm × 9.5 nm constant-current STM image of a pentacene molecule bound to a herringbone kink of the reconstructed Au(111) surface. The inset shows the apparent height profile taken along this pentacene molecule. Scanning conditions: $I = 45$ pA, $V = 100$ mV.

since this is a favorable adsorption site, and the molecule is unlikely to move while scanning. During this dI/dV data acquisition process, using standard lock-in detection techniques [6], the feedback loop is kept active in order to maintain the tunneling current at a constant preset value. Topographic and dI/dV signals are acquired at each (x, y) pixel, with the z value being acquired before the dI/dV signal.

To ensure that STM tips are clean and suitable for dI/dV measurements on a single molecule, differential conductance spectra were first recorded on bare Au(111) terraces. Only those tips capable of yielding signatures in spectra corresponding to the Au(111) surface state at ~ -505 mV were utilized [7]. Figure 2(a) shows a typical dI/dV spectrum recorded on a pentacene molecule physisorbed on a herringbone kink. Distinct from the Au(111) surface state, it presents several conductance peaks at -900 mV, -1900 mV, and -2700 mV and an additional broad peak at $+1300$ mV.

Constant-current STM images of a single pentacene molecule taken at these dI/dV peaks show an intramolecular spatial modulation along the pentacene axis, as shown in the left column of Fig. 2(b). These features gradually fade out at higher voltages, while images recorded at bias voltages close to the Fermi level (see Fig. 1) show no internal features. This modulation is smaller in amplitude when compared with STM images reported by Repp *et al.* [2] for pentacene adsorbed on a NaCl decoupling layer. The number of maxima along the pentacene axis in the image recorded at -900 mV corresponds to the electron probability distribution of the HOMO of a pentacene molecule in the gas phase. This -900 mV peak measured with respect to the Fermi level corresponds to an electronic resonance located at -6.25 eV with respect to the vacuum level, since the Au(111) work function is 5.35 eV. Therefore this resonance can be identified as the 6.6 eV first ionization potential of a free pentacene molecule. The minor discrepancy in energy, compared to 6.6 eV, can be attributed to a renormalization of molecular levels caused by the adsorption of the pentacene on the Au(111) metal surface [5,8]. Here, the tunneling process through the pentacene molecule at -900 mV is able to capture the HOMO as the main orbital component of its first ionized state resonance contributing to the STM tunnel junction conductance. This is not the case for a pentacene chemisorbed on Cu(111) as reported by Lagoute *et al.* [9]. In Fig. 2(b) intramolecular modulations are also observed in the topographic images recorded at -1900 mV, at -2500 mV, and very weakly at $+1300$ mV. The 1300 mV corresponds to the first reduced state of the pentacene, whose electron affinity lies at 1350 mV [10].

To disentangle those monoelectronic MO contributions from the intramolecular spatial variation of the STM junction conductance, constant-current differential conductance images of a pentacene molecule were acquired at different voltages in the range between -2.5 and 1.3 V,

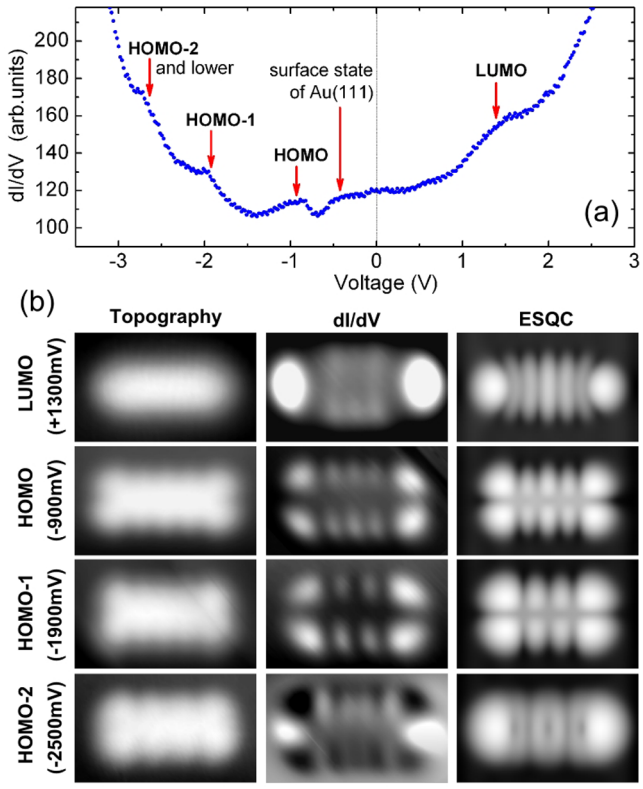

FIG. 2 (color online). (a) The dI/dV spectrum of a pentacene molecule on Au(111). The dI/dV signal shows four broad and distinct peaks corresponding to the first affinity level (LUMO) of a pentacene, in the positive bias side, and its one electron ionization levels (HOMO, HOMO-1, and lower) in the negative side. The leftmost peak certainly consists of two resonances, HOMO-2 and HOMO-3, but these are too close energetically to be resolved by spectroscopy in this high voltage region [13]. The surface state of Au(111) is also observable. (b) The left and center columns are experimental topographic images and dI/dV maps recorded at voltages indicated by the arrows in (a). Tunneling currents for the STM images and dI/dV maps are, from the top, 5 nA, 3 nA, 5 nA, and 6 nA. The right column displays the corresponding calculated STM-elastic scattering quantum chemistry (ESQC) images, at a constant tunneling current of 1 nA, for a pentacene molecule adsorbed on Au(111) at the monoelectronic energy resonances corresponding to the LUMO, HOMO, HOMO-1, and HOMO-2, respectively. All images are 2.5 nm $\times$ 1.5 nm.

including the characteristic dI/dV peaks shown in Fig. 2(a). At a given position (x, y) and for a tip apex to surface distance z, I is given by

$$I(V, z) = \frac{e^2}{\pi\hbar} \int_{E_F}^{E_F + eV} T(E, z) dE, \qquad (1)$$

where $T(E, z)$ is the electronic transparency of the tunnel junction at energy E. To visualize the corresponding MOs' electron probability distribution, the dI/dV map was recorded at constant current. To a first order approximation, $T(E, z)$ is simplified to

$$T(E, z) \propto C_{\text{eff}}^2(E, z)\Delta\rho(E), \quad (2)$$

where $C_{\text{eff}}(E, z)$ is the effective interelectrode electronic coupling through the molecule, and $\Delta\rho(E)$ is the differential change in the metal surface local density of states caused by the molecule interacting with the surface. For a physisorbed molecule, the local density of states do not vary significantly around a given molecule resonance, and the dI/dV corrugation depends only on $C_{\text{eff}}(E, z)$. For any (x, y) where the tip apex is well coupled to the electronic cloud of the molecule, the constant-current condition leads to a tip retraction. The corresponding $T(E, z)$ resonance width is reduced by this decrease in $C_{\text{eff}}(E, z)$, and large spatial variations in dI/dV result. In contrast, at (x, y) positions where the apex is weakly coupled, the tip approaches the molecule, the $T(E, z)$ resonances broaden, and the dI/dV is reduced. Since the tunneling current is mainly formed by a succession of temporally uncorrelated one electron transfer events through the molecule [11], the main coupling contribution to $C_{\text{eff}}(E, z)$ is the monoelectronic coupling term through the corresponding MO energy level. The experimental constant-current dI/dV maps are presented in the center column of Fig. 2(b). The maps recorded at -900 mV and -1900 mV are similar to the free pentacene electron probability distribution of HOMO and HOMO-1, respectively. Here, the variations of $C_{\text{eff}}(E, z)$ sample the single electronic contributions to the Slater determinant of the electronic cloud. While nonresonant MO contributions in this determinant are filtered through the molecule, the spatial extent of each experimental MO image differs from two-dimensional maps of a free pentacene molecule π orbitals, calculated either by semiempirical [3] or density-functional theory [2] methods, especially at the ends of the molecule. It is the electronic interaction of the π MO with the tip which creates the apparent lateral expansion and enlargement at the molecule extremities. A more realistic way to compare experimental and calculated images is to use the elastic scattering quantum chemistry (ESQC) calculation technique and to compute a map of STM tip height (z map) for a constant current exactly at the imaged MO energy [12]. Since ESQC employs a single electron Hamiltonian, the calculated images presented at the right column of Fig. 2(b) are identical to the experimental ones, after including the tip effect.

The dI/dV image recorded at $+1300$ mV shows a clean contribution of the monoelectronic LUMO state of the corresponding Slater determinant of this resonance as confirmed by the full STM-ESQC constant-current dI/dV image calculation. However, there are differences for HOMO-2, which are explained below.

A consequence of our imaging technique is that dI/dV remains sensitive to the spatial variations of $C_{\text{eff}}(E, z)$ even away from a resonance. For example, the dI/dV image in Fig. 3(b) recorded at -1400 mV in between the HOMO-1 and HOMO-like resonances is essentially the negative of the HOMO image presented in Fig. 2(b), despite the absence of MO traces in the normal topographic image [Fig. 3(a)]. This indicates that for energies lower than the HOMO, $C_{\text{eff}}(E, z)$ remains sensitive to its monoelectronic contribution until a second electronic state attributed to the HOMO-1 single electron resonance occurs. At -1400 mV, and at the (x, y) position of a HOMO spatial maximum, the STM tip is retracted to maintain constant current. Therefore, in the absence of any resonance at nearby energy, this retraction renders dI/dV very small, explaining the dark contrast HOMO-like lobes in Fig. 3(b). In contrast, at the (x, y) position of a HOMO node and also away from the molecule, the feedback loop makes the tip approach, and the dI/dV signal is larger than at a MO maximum lobe position. This indicates that the resonances observed in this manner are not purely single electronic resonance.

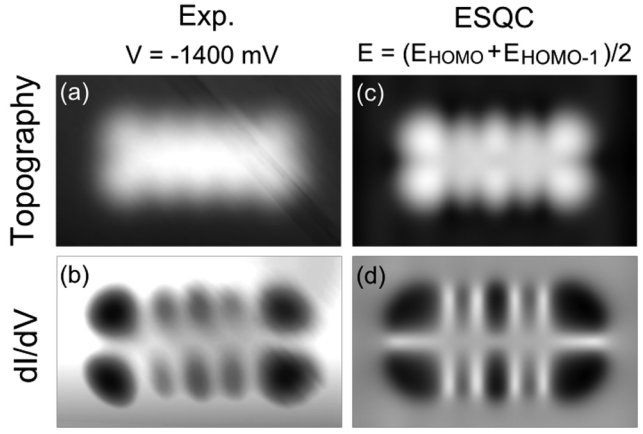

FIG. 3. (a) Topographic and (b) dI/dV images taken in the gap between the HOMO and HOMO-1 resonances ($V = -1400$ mV and $I = 4$ nA). (c) Constant-current ESQC-computed z map, at 1 nA. Here the integration performs from the Fermi energy to an energy lying exactly midway between the HOMO and HOMO-1. (d) ESQC-computed conductance map at $E = (E_{\text{HOMO}} + E_{\text{HOMO}-1})/2$ using the z map shown in (c). All images are 2.5 nm $\times$ 1.5 nm.

Using the local tip apex interaction with the electronic cloud of the molecule, the tunneling current picks up selected monoelectronic eigenstates of the electronic cloud. This highlights the contributions of the HOMO and LUMO, as shown in Fig. 2(a). We have used a modified version of the STM-ESQC technique to reproduce this negative image of the HOMO single electron state. The STM image was calculated in a constant-current mode after including Eq. (1) in ESQC for calculating the feedback current, instead of its usual linear approximation. This image is presented in Fig. 3(c). This z map was then used to get the corresponding dI/dV image just by calculating a new $T(E, z)$ ESQC map according to the derivative of Eq. (1). This image is presented in Fig. 3(d) for $E = (E_{\text{HOMO}} + E_{\text{HOMO-1}})/2$ relative to the Fermi level. The

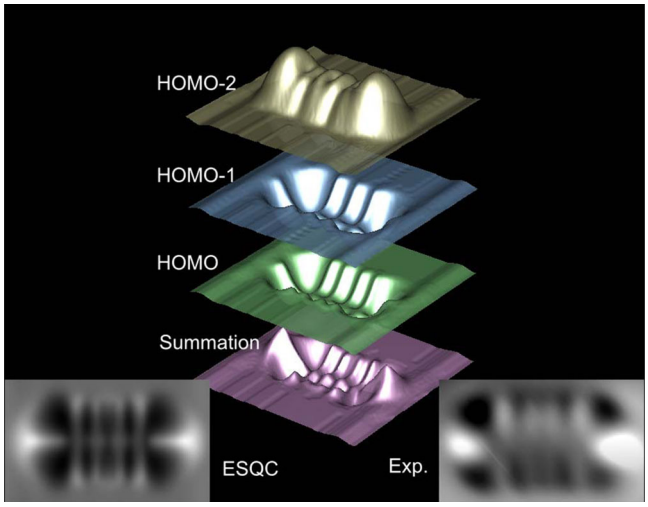

FIG. 4 (color online). A three-dimensional (3D) representation showing the contribution of resonant and nonresonant states explaining the dI/dV map recorded at -2500 mV. The three topmost 3D plots were extracted from the ESQC theoretical results shown in the right column of Fig. 2(b). The 3D plot at the bottom corresponds to the weighted sum of the HOMO-2, HOMO-1, and HOMO shown above. The criteria for the integration is (i) resonant states (HOMO-2 in this case) are positive, (ii) nonresonant states (HOMO and HOMO-1) are negative, and (iii) the nearer the Fermi energy, the stronger is the contribution of the nonresonant states [14]. The image at the bottom-left corner shows the top view of the integrated 3D plot, and the bottom-right image is the corresponding experimental dI/dV map.

agreement with the experimental dI/dV map shows that the tip captures $C_{\mathrm{eff}}(E, z)$ spatial variations of the active monoelectronic orbital in the electron transfer process at $E = -1400$ meV through the molecule. The HOMO-1 contribution does not appear here because the energy window has not reached its corresponding electronic cloud resonance to activate the next one electron transfer channel.

Another consequence is that at higher voltages (for example, -2500 mV), dI/dV images are composed of a very complex intermixing of positive (for example, the corresponding HOMO-2 contribution) and negative (the previous out-of-resonance MOs' contributions) lobes. At -2500 mV, the monoelectronic contributions discussed earlier are still active in the tunneling process but uncorrelated. They are superposed on the main HOMO-2 contribution corresponding to the one electron ionization process detected at the -2500 mV resonance. A reconstruction of the dI/dV map recorded at -2500 mV is proposed in Fig. 4. Each of the HOMO-2, HOMO-1, and HOMO contributions was inverted and weighted as necessary. The HOMO-2 MO is present but overshadowed by the two other MOs.

In conclusion, our constant-current dI/dV image technique is able to image the principal monoelectronic MO contributions of the one electron ionized and reduced states of the pentacene π electron cloud on a bare metal surface. The usual nomenclature used in STM spectroscopy on molecules can be preserved, with the caveat that experimental images attributed to a MO are only an approximate description of the real electron cloud. All molecules may not show such a clear correspondence between their STM dI/dV images at single electron states and the spatial distribution of the electron cloud at ionized or reduced states of the free molecule.

We acknowledge the Agency for Science, Technology, and Research (A*STAR) for funding provided through the Visiting Investigatorship Program (phase I) ''Atomic Scale Technology Project.''

[1] T. Koopmans, Physica (Amsterdam) **1**, 104 (1934).
[2] J. Repp, G. Meyer, S. M. Stojković, A. Gourdon, and C. Joachim, Phys. Rev. Lett. **94**, 026803 (2005).
[3] C. J. Villagomez *et al.*, Chem. Phys. Lett. **450**, 107 (2007).
[4] Y. Makoudi *et al.*, Phys. Rev. Lett. **100**, 076405 (2008).
[5] J. B. Neaton, M. S. Hybertsen, and S. G. Louie, Phys. Rev. Lett. **97**, 216405 (2006).
[6] R. S. Becker, J. A. Golovchenko, D. R. Hamann, and B. S. Swartzentruber, Phys. Rev. Lett. **55**, 2032 (1985).
[7] W. Chen, V. Madhavan, T. Jamneala, and M. F. Crommie, Phys. Rev. Lett. **80**, 1469 (1998).
[8] S. K. M. Henze, O. Bauer, T.-L. Lee, M. Sokolowski, and F. S. Tautz, Surf. Sci. **601**, 1566 (2007).
[9] J. Lagoute, K. Kanisawa, and S. Fölsch, Phys. Rev. B **70**, 245415 (2004).
[10] L. Crocker, T. Wang, and P. Kebarle, J. Am. Chem. Soc. **115**, 7818 (1993); G. Malloci, G. Mulas, G. Cappellini, V. Fiorentini, and I. Porceddu, Astron. Astrophys. **432**, 585 (2005).
[11] C. Joachim and M. A. Ratner, Proc. Natl. Acad. Sci. U.S.A. **102**, 8801 (2005).
[12] P. Sautet and C. Joachim, Chem. Phys. Lett. **153**, 511 (1988); P. Sautet and C. Joachim, Phys. Rev. B **38**, 12 238 (1988).
[13] The conductance of a pentacene molecule in a tunnel junction constituted by gold electrodes computed by ESQC shows resonant peaks at -10.51, -11.36, -12.24, -12.60, and -12.84 eV as LUMO, HOMO, HOMO-1, HOMO-2, and HOMO-3, respectively. The energy difference of HOMO-2 and HOMO-3 is relatively small compared to others.
[14] The tunneling probability of electronic states included within this energy range decays monotonically with their energy, meaning that electronic states closer to the Fermi level have a higher tunneling probability than those closer to E_{Bias}.